

Post-deposition processing options for high-efficiency sputtered CdS/CdTe solar cells

Naba R. Paudel,¹ Matthew Young,² Paul J. Roland,¹ Randy J. Ellingson,¹ Yanfa Yan,¹ and Alvin D. Compaan¹

¹*Department of Physics & Astronomy, University of Toledo, Toledo, Ohio 43606, USA*

²*National Renewable Energy Laboratory, Golden, Colorado 80401, USA*

(Received 30 October 2013; accepted 25 January 2014; published online 10 February 2014)

CdCl₂ activation near 400 °C is known to be critically important for obtaining high efficiency CdS/CdTe solar cells. However, this treatment step behaves differently on high-temperature-grown CdTe than on lower-temperature-grown CdTe layers such as those grown by sputtering. On sputtered films, the post-deposition activation produces grain-boundary passivation, sulfur diffusion into CdTe, and substantial grain growth. Nevertheless, we find the CdCl₂ process for sputtered films to be characterized by a single activation energy that we interpret as applying to S diffusion into CdTe. We find this activation energy to hold for CdCl₂ treatments from 370 to 440 °C. The completed CdS/CdTe solar-cell structures showed somewhat poorer initial performance with activation above 420 °C, but, in this case, the cell efficiency increased after accelerated life testing at 85 °C, open-circuit biasing and one-sun illumination. With an optimized CdCl₂ activation process, the use of oxygenated sputtered CdS, and low-iron soda-lime glass, cell efficiencies of 14.5% were achieved. © 2014 AIP Publishing LLC. [<http://dx.doi.org/10.1063/1.4864415>]

I. INTRODUCTION

Polycrystalline CdS/CdTe films typically need to be activated with CdCl₂ vapor and partial pressures of oxygen at 350–450 °C to obtain the highest efficiency.¹ This special heat treatment step, often called activation (or chloride activation), is routinely used in the device fabrication process for the highest efficiency CdTe solar cells. This activation step appears to be even more effective for films grown at 300 °C or lower such as by sputtering and is thought to facilitate several mechanisms: CdS_xTe_{1-x} alloying,^{2,3} recrystallization with random growth orientation,^{4,5} increase in the density of the acceptor complex (V_{Cd}Cl_{Te}),^{6,7} grain-boundary passivation, and enhancement of the minority carrier lifetime.⁸ With the aid of such mechanisms, the CdS/CdTe cells collect more photocurrent and show increased open-circuit voltage and fill factor such that significantly improved efficiencies can be achieved over as-grown cells.^{8,9}

The optimization of post-deposition activation parameters is especially delicate and critical for low-temperature growth. For instance, our group has typically used 30 min activation at 387 °C as a standard activation condition for 2.1 μm thick sputtered CdTe solar cells.^{10–12} In this study, our main focus is to understand the fundamental aspects of activation for sputtered CdS/CdTe films and identify whether a simple Arrhenius behavior (with a single activation energy) applies to these fine-grain polycrystalline films. Our procedure, in this study, was to apply the activation step over a large range of temperatures and focus on analyzing morphological changes and the S-diffusion into the sputtered CdTe film. We explore a very short activation step for sputtered cells using temperatures well above 400 °C in a regime often called “rapid thermal annealing” and compare the cell

performance and the resulting cell stability with our standard activation condition. Because of the shorter activation step, this higher-temperature regime may be especially cost-effective for high-speed production.

II. EXPERIMENTAL DETAILS

Thin films of 80 nm thick CdS and 2.1 μm thick CdTe were sputtered on standard SnO₂:F/SnO₂ coated low-iron soda-lime glass substrates provided by NSG, North America, with details described elsewhere.^{12,13} The as-grown samples then received the wet method of chloride activation (a saturated CdCl₂/methanol solution applied directly to the CdTe surface) with a variation in annealing temperature (370 °C–440 °C) and activation time from less than 1 min to 2 hrs. Shorter activation times were used for the higher temperatures consistent with the expected Arrhenius behavior of the S and Cl diffusion.¹⁴ For each temperature, the activation time was varied to yield best solar cell performance. The as-grown and activated samples were analyzed using Secondary Electron Microscopy (SEM), X-ray Diffraction (XRD), Secondary Ion Mass Spectroscopy (SIMS), and Time-resolved Photoluminescence (TRPL) techniques. Prior to the back-contact application, the activated samples were rinsed a few times with methanol. Bilayer metallic contacts: Cu (3 nm) and Au (20 nm), were then thermally evaporated through thin metal masks followed by 45 min of diffusion at 150 °C in air. To achieve statistically significant results, at least 20 dot cells of 0.12 cm² were prepared for each activation condition. For accelerated life testing (ALT), CdTe cells either received 300 hrs of damp heat testing (85 °C/85% relative humidity (RH)) or light soaking at 85 °C in air under one-sun illumination and V_{OC} biasing.

III. RESULTS AND DISCUSSIONS

A. Effect of CdCl_2 activation on sputtered CdS/CdTe films

In contrast with high-temperature CdTe, deposited, e.g., by vapor transport deposition or closed space sublimation, the activation step has large effects on the surface morphology of sputtered CdTe films as seen in the plan-view secondary electron micrographs shown in Figures 1(a) and 1(b). The activation step recrystallizes the CdTe film and alters the grain size, grain orientation, and grain morphology. We observed highly faceted and compact grains with a substantial increment in lateral dimension after providing the standard activation. The increase is typically by a factor of 2 to 5. Using *ImageJ*,¹⁵ the average grain size is estimated as 340 ± 120 nm for as-deposited CdTe films and 750 ± 210 nm after post-deposition chloride activation.

As-sputtered CdTe films generally exhibit strong orientation along the $\langle 111 \rangle$ direction with texture coefficient 6.2.¹⁶ With CdCl_2 activation, the x-ray diffraction spectra shown in Figure 2(a) indicate nearly random grain orientation with the texture coefficient decreasing to 2.0 indicating significant grain regrowth. The recrystallization decreases the broadening of the characteristic peaks implying grain growth as observed in SEM results.

Alloying that produces a $\text{CdS}_x\text{Te}_{1-x}$ layer is another major outcome of the activation step for sputtered CdS and CdTe films; the alloying can be analyzed using high-angle x-ray diffraction as used by McCandless *et al.*² As shown in

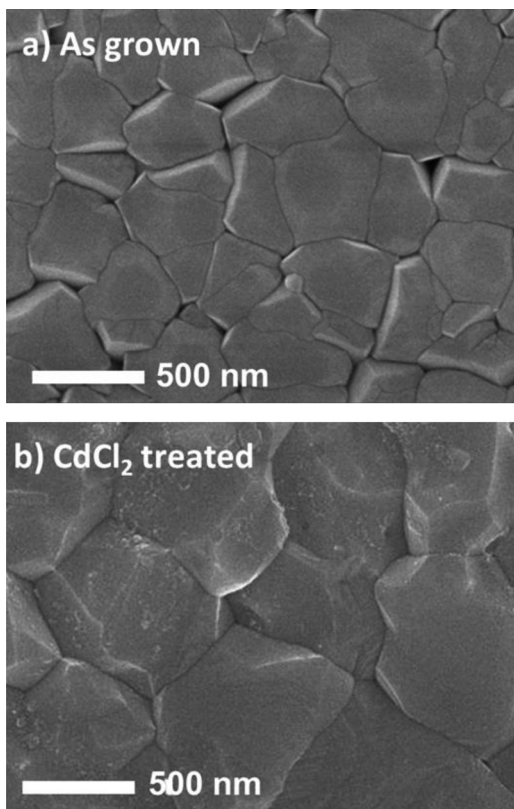


FIG. 1. SEM micrographs of sputtered CdS/CdTe films grown on SnO_2 :F/ SnO_2 -coated soda-lime glass substrates; (a) as grown (b) after 30 min activation at 387°C in dry air and chloride vapor.

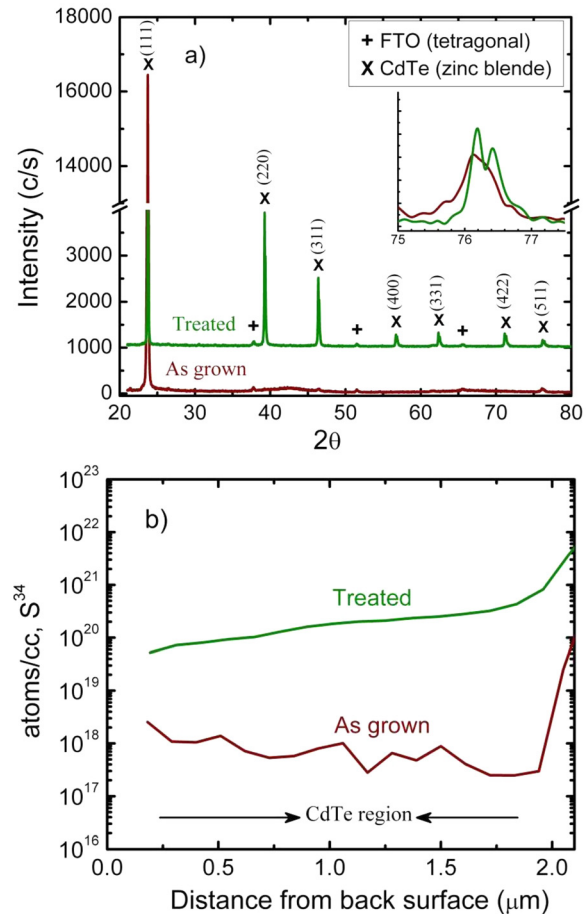


FIG. 2. (a) X-ray diffractograms and (b) SIMS depth profiles of the sputtered CdS/CdTe films grown on SnO_2 :F/ SnO_2 -coated soda-lime glass substrates before and after 30 min activation at 387°C in dry air and chloride vapor.

the inset of Figure 2(a), the double peak along the $\langle 511 \rangle$ direction is consistent with a S-alloyed region in CdTe with about $\sim 0.2\%$ smaller lattice constant. As-grown sputtered films exhibit no interdiffusion since the growth temperature is less than 300°C ; however, the broad peak indicates very small grain size. The alloying is further verified with the SIMS concentration depth profile shown in Figure 2(b). The depth profiles were performed on a Cameca IMS-5f Secondary Ion Mass Spectrometer using a Cs⁺ primary ion source. The samples were biased at -4.5 kV. From the SIMS data, the concentration of sulfur in the CdTe region for the as-sputtered film is barely detectable at about 10^{18} cm^{-3} , which is less than 0.01% of the sulfur density in CdS ($2 \times 10^{22} \text{ cm}^{-3}$). After the activation step, sulfur diffuses out from the CdS region decreasing from an average of about 10^{21} cm^{-3} at the CdTe interface to about 10^{20} cm^{-3} near the back surface. The S concentration will be much higher near the grain boundaries due to much higher grain boundary diffusion so the SIMS data only represent average values at each depth. The distinct higher-angle $\langle 511 \rangle$ peak at 76.4° indicates an S concentration of about 3% or $\sim 6 \times 10^{20} \text{ cm}^{-3}$.² This likely arises mostly from more heavily alloyed regions around the grain boundaries.

In order to explore the carrier lifetime of the CdTe films, TRPL was performed at room temperature for both as-grown

and chloride-activated CdS/CdTe samples. The free CdTe film surface was photo-excited by a 20 MHz pulsed laser at 633 nm, and the photoluminescence was detected at 825 nm; the instrument response function (IRF) was determined using an 825 nm pulsed laser and a scattering target. An estimated laser spot size of $130 \pm 5 \mu\text{m}$ and incident pulse energy of 1.4 pJ/pulse yields a photo-induced carrier concentration of approx. 3.8×10^{15} . Minority carrier lifetimes were extracted by re-convolution of a bi-exponential with the IRF to obtain a least-square best fit.¹⁷ Figure 3(a) shows the decay function before (as-grown) and after chloride activation. The fast decay time, τ_1 , increases from 63 ps to 154 ps after activation; the slow decay component, τ_2 , is not distinguishable prior to activation but is 1.23 ns after the 30-min CdCl₂ activation step. In contrast, through-the-glass measurements (following activation) at the CdS/CdTe junction indicated decay lifetimes of $\tau_1 = 491$ ps and $\tau_2 = 5.1$ ns. The carrier lifetimes measured here agree well with those reported by other groups when using the single-photon-excitation (IPE) method.^{18,19} We attribute the significant improvement in lifetime for our sputtered devices to several factors including an improvement in CdTe grain size, optimum interdiffusion,

grain boundary passivation, and reduction of the density of point defects within the grains.

Solar cell structures, completed with the application of our standard Cu/Au contacts, exhibited remarkable improvements in short-circuit current (J_{SC}), open-circuit voltage (V_{OC}), fill factor (FF), efficiency (Eff), series resistance (R_{S}), and shunt resistance (R_{SH}). The as-grown device showed much poorer cell performance: $V_{\text{OC}} = 372$ mV, $J_{\text{SC}} = 0.8$ mA/cm², FF = 32.2%, and Eff = 0.1%, compared with the activated cell: $V_{\text{OC}} = 831$ mV, $J_{\text{SC}} = 22.7$ mA/cm², FF = 72.2%, and Eff = 13.6%. With chloride activation, the series resistance decreases by almost a factor of 100. This is likely due both improved mobility and an increase in hole density due to increased Cu concentration after activation (indicated by SIMS data not shown here). The activation also is known to provide grain boundary passivation. As a result, a major increase in carrier collection was realized. The light J-V data of the as-sputtered cell plotted in Figure 3(b) show an almost ohmic behavior indicating that the CdTe absorber layer is very resistive without chloride activation even though the back contacts were made with the standard Cu/Au deposition and diffusion.

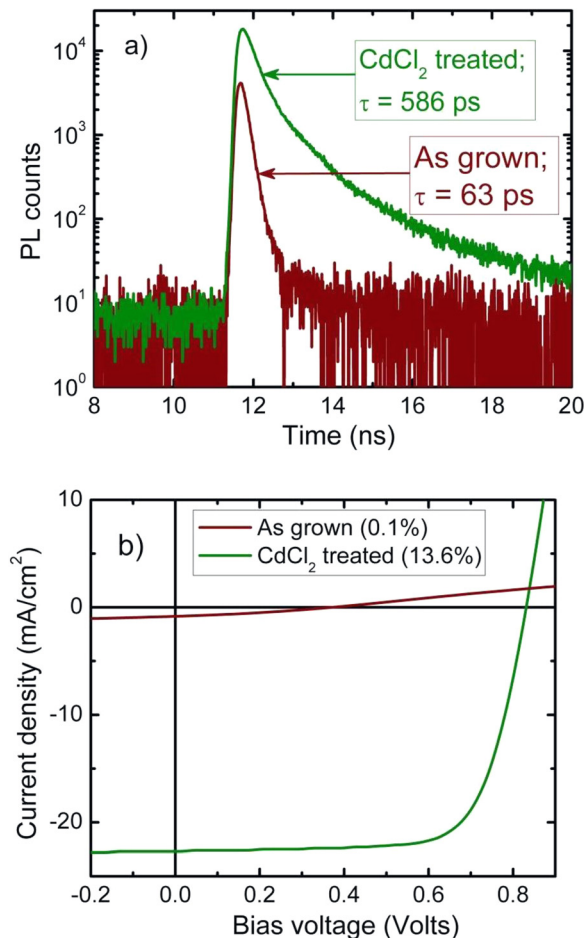


FIG. 3. (a) Time-resolved photoluminescence spectra and (b) light J-V characteristics of sputtered CdS/CdTe cells grown on SnO₂:F/SnO₂-coated soda-lime glass substrates before and after 30 min activation at 387 °C in dry air and chloride vapor. (Note: For J-V measurements, the devices were completed with the application of Cu/Au back contacts and 150 °C diffusion.)

B. Effects of high and low temperature activation

To determine optimum chloride activation with temperatures from 370 °C to 440 °C, the sputtered CdS/CdTe devices were activated for various times at each temperature and the best value chosen from the cell performance results. The best devices at each temperature were again evaluated by x-ray diffraction. The x-ray spectra of three representative samples presented in Figure 4(a) show that all optimized films had almost random grain orientation after CdCl₂ activation; however, the optimized treatment time was much shorter at the higher temperatures. For example, a 20 s treatment was optimum at 440 °C vs. 80 min at 370 °C. The peak intensity of the XRD profiles at optimized duration was comparable whether the treatment was done at 370 °C or 440 °C.

CdS and CdTe intermixing was studied with a narrow-angle scan across the (511) peak as shown in Figure 4(b). The higher angle peak (smaller lattice constant) observed in the doublet features is the signature of CdS_xTe_{1-x} alloying, where the lower angle peak is from the pure CdTe reflection. Among eight samples, the activation provided at 410 °C has a somewhat longer shoulder on the high angle side of the 2nd peak indicating stronger intermixing. Correspondingly, the pure CdTe signal was suppressed for this sample. Using the approach described by McCandless *et al.*,² we estimated $x = 2.0 \pm 0.3\%$ alloying of CdS_xTe_{1-x} layers for all treatment temperatures that optimized the sputtered CdTe cells.¹⁶ The XRD result also well agrees with SIMS measurement shown in Figure 2(b) when we consider average sulfur concentration of entire 2.1 μm thick CdTe layers.

To identify the optimum activation conditions, we varied the activation time from less than 1 min to as much as 2 hrs at temperatures from 370 °C to 440 °C. After the activation step, CdS/CdTe devices were completed by evaporating Cu (3 nm)/Au (20 nm) dots and the cell performances were

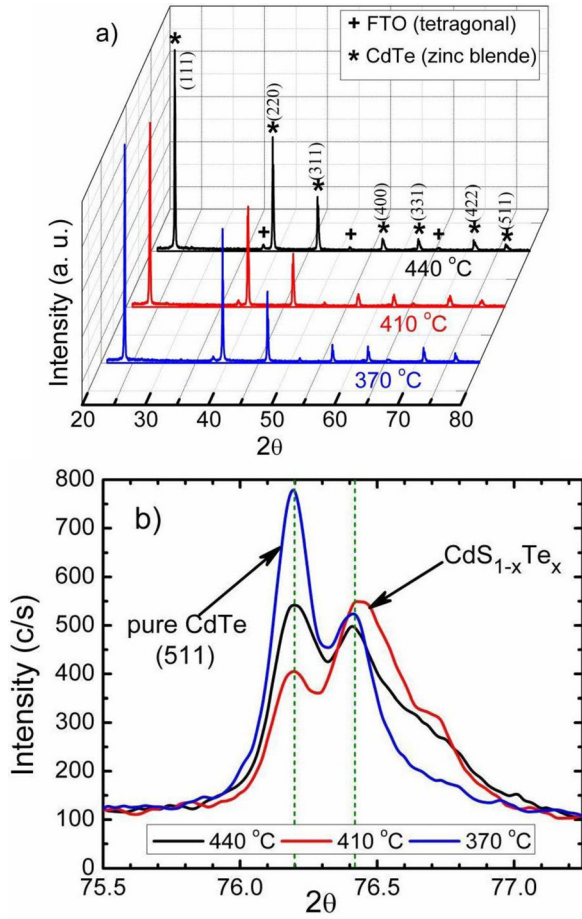


FIG. 4. (a) X-ray diffractograms of sputtered CdS/CdTe films on HRT-coated SnO_2/F glass substrates after post-deposition activation at 370 °C, 410 °C, and 440 °C. (b) Narrow angle scan across (511) peak of CdTe sample described in Figure 4(a).

measured. Figure 5 shows the activation time determined as optimum for each treatment temperature. The average cell efficiency of 20 dot cells at each temperature as a function of activation temperature after optimization of their treatment

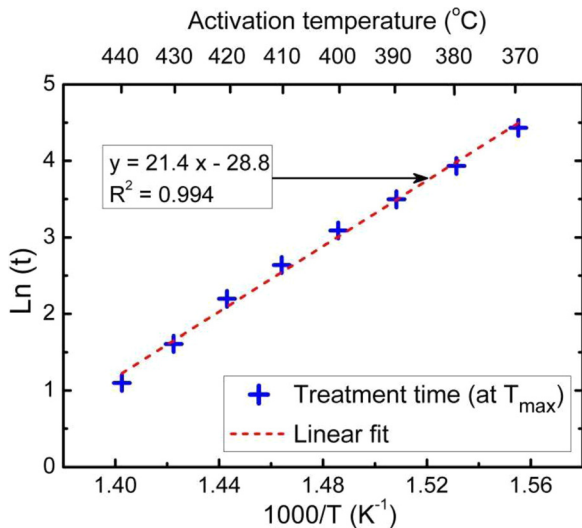


FIG. 5. $\ln(t)$ vs. $1000/T$; where “ t ” is optimum activation time at the T_{\max} , which did not include ramp-up and cool-down period. Dashed line follows Eq. (3) with $E_a = 1.84$ eV.

time is shown in Figure 6(a). It should be pointed out that the activation time described here was the actual time spent by the CdTe sample at the set point temperature. Since we used very short ramp-up ($3^\circ\text{--}4^\circ$ per second) and cool-down ($\sim 2^\circ$ per second) times, such periods were not included in our activation time; these make small contributions to the activation process. As expected but not shown here, higher J_{SC} was realized at higher activation temperature, when activation time was kept the same, indicating stronger S diffusion into the CdTe producing a red-shift of the $\text{CdS}_x\text{Te}_{1-x}$ band edge. But this over-treatment appears to lead to more compensating defects in CdTe and results in poorer V_{OC} and FF. CdTe cells exhibited nearly 13% average efficiency when the activation temperature was at 370 °C and the time optimized but the efficiency optimized at only 11.3% for 440 °C (Figure 6(a)). This could be related to a poorer interface formation at CdS/CdTe junction and poor electrical properties of CdTe due to increased defects. More specifically, the solar cells exhibited poorer FF and V_{OC} above 400 °C activation although the J_{SC} of these cells are comparable. At optimum conditions, the activation time decreases exponentially as temperature increases (Figure 5), which confirms an Arrhenius relationship between “ $1/t$ ” and “ T .”

C. Estimation of activation energy for sulfur diffusion

As discussed above, when CdS and CdTe films are grown at less than 300 °C substrate temperature, little interdiffusion occurs. But the post-deposition activation step performed in the presence of Cl and O drives a significant amount of sulfur into the CdTe region as evidenced by the SIMS profile shown in Figure 2(b). Based on this approach, we have modeled the optimized activation parameters to calculate the activation energy for S diffusion in CdTe. Note that we have used optimum cell performance as the figure of merit. Factors other than S diffusion certainly contribute to optimum cell performance, including grain boundary passivation, grain orientation, grain growth, hole concentration, and minority carrier lifetime. However, since the efficiency and the secondary cell performance parameters (V_{OC} , J_{SC} , and FF) all optimize at similar values, we assume that the optimum cell performance always occurs at the same S profile for the different temperatures. This gives us the reference point we need to follow the temperature-time relationship of the sulfur diffusion.

According to the kinetic theory of diffusion, the characteristic diffusion length is, $l = 2\sqrt{D(T)t}$, where “ D ” is the diffusion coefficient and “ t ” is the diffusion time.²⁰ This equation is valid for one-dimensional diffusion from a source of constant concentration. We assume that the n-type CdS window layer is an infinite source of constant concentration for sulfur diffusion and the thickness of the CdTe absorber layer ($\sim 2\ \mu\text{m}$ for our cells) is the characteristic length for our device structure. With these assumptions, the diffusion time can be expressed as inversely proportional to the diffusion coefficient $D(T)$

$$t \propto \frac{1}{D(T)}. \quad (1)$$

Since the diffusion coefficient typically has an “activated” behavior, it can be written as²⁰

$$D(T) = D_0 \exp\left(\frac{-E_a}{K_B T}\right). \quad (2)$$

Thus, from Eqs. (1) to (2), one has

$$\frac{1}{t} = \frac{1}{C_0} \exp\left(\frac{-E_a}{K_B T}\right), \quad \text{Ln}(t) = \frac{E_a}{K_B T} + \text{Ln}(C_0), \quad (3)$$

where “ C_0 ” is a proportionality constant depending on several physical properties of the material such as diffusion coefficient, the characteristic diffusion length as well as the partial pressure of Cl used but this will change with temperature. In order to obtain the activation energy, we replaced the diffusion time by the optimized activation time “ t ” and plotted $\text{Ln}(t)$ vs. $1000/T$ shown in Figure 5. The linear fitting of these data points follows the relation expressed in Eq. (3) with $E_a = 1.84 \pm 0.05$ eV, which is close to the value of 1.9–2.0 eV reported by McCandless *et al.*² and Lane *et al.*²¹ This activation energy corresponds to grain boundary diffusion, which will dominate over bulk intra-grain diffusion. The slightly lower activation energy we obtained in this study is most likely due to the smaller grains and higher density of grain boundaries produced during magnetron sputtering than the high temperature growth processes of Ref. 2.

D. Accelerated life testing of high temperature activated cells

To further understand the role of the activation temperature on the performance of sputtered CdS/CdTe cells, devices that received activation at 440 °C and 430 °C were subjected to accelerated life testing (ALT) for 300 hrs either using light soaking (under 1 sun illumination) at 85 °C or damp heat testing at 85 °C/85% RH. Unlike devices activated at 390 °C,¹² CdTe cells activated at higher temperature showed improvements in FF and V_{OC} during both ALTs without losing short-circuit current. An average of 65% fill factor and 780 mV open-circuit voltage was measured on virgin cells immediately after high temperature activation. After 300 hrs of ALT, the cells showed enhancement in FF to 70% and V_{OC} to 820 mV. Therefore, the average cell efficiency also improved to well above 13%, as shown in Figure 6(a). Compared with the damp-heat-stressed cells (activated at 430 °C), light-soaked cells (activated at 440 °C) exhibited somewhat more improvement indicating that the one-sun illumination is advantageous for improving the cell performance. It should also be noted that sputtered CdS/CdTe cells which received the standard activation (390 °C, 30 min.) had initially higher performance than the high temperature activated cells but exhibited lower performances after ALT. Thus, although sputtered CdTe cells activated at higher temperature showed poorer initial performance, they ended up with slightly better efficiency (especially after light soaking test) than devices with the standard chloride treatment, shown in Figure 6(a). We speculate that the ALT at 85 °C after high temperature activation compensates some of the point defects introduced at the high temperature, enhancing the electrical properties and yielding better interfaces. However, further study is

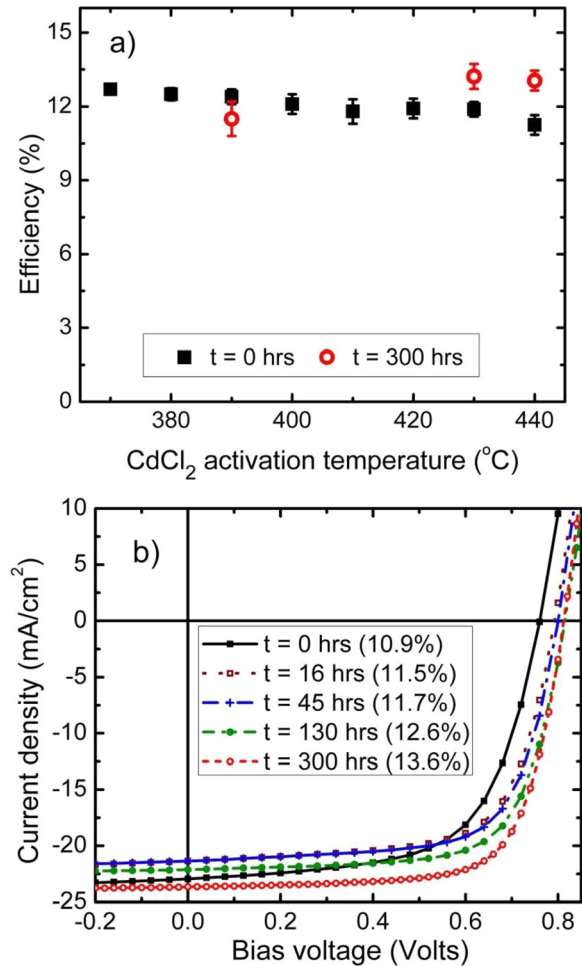


FIG. 6. (a) Average efficiency of 20 sputtered CdS/CdTe dot cells as a function of activation temperature before and after receiving 300 hrs of accelerated life testing. The stressing was performed at 85 °C, at open-circuit bias and under 1 sun illumination (for light soaking) and with 85% relative humidity (for damp heat test). (b) Light J-V of the light-soaked cell measured after several hours of ALT.

needed to confirm these inferences, which will be also helpful to understand the micro-structural changes that occurred during high temperature activation and ALT.

The light J-V data from cells that received only 20 s activation at 440 °C, taken after several hours of light-soaking, are shown in Figure 6(b). The cells showed noticeable improvement in FF and V_{OC} already after 16 hrs of ALT. The solar cell efficiencies further improved with ALT up to 300 hrs.

E. High efficiency sputtered CdS/CdTe cells on soda-lime glass with CdS:O

Sputter deposition provides low energy ion and electron bombardment during thin-film growth, which facilitates control of deposition rate and grain size. Compared with high-temperature sublimation or vapor transport methods,^{2,22,23} this low-temperature method yields relatively smaller grains, almost an order of magnitude smaller. So far the reported highest cell efficiency of sputtered CdS/CdTe cells is 14%.²⁴ This efficiency was obtained while using 1 mm thick aluminosilicate glass substrates (ASG) with aluminum-doped zinc oxide (AZO) front contacts. ASG with AZO has better light

transmission and higher J_{SC} than commercial fluorine-doped tin oxide (FTO) front contact layers on 3.2 mm thick standard soda-lime glass.

Here we also report progress towards increased efficiency of sputtered cells with the use of $\text{SnO}_2:\text{F}/\text{SnO}_2$ coated low-iron soda-lime glass substrates with a high resistivity transparent (HRT) layer supplied by NSG, NA. With careful optimization of our fabrication process that also includes modification of the CdS window layer, we have achieved cell efficiencies of nearly 14.5% without antireflection coating. The other performance parameters of our small-area (0.08 cm^2) cell are: $V_{OC} = 847 \text{ mV}$, $J_{SC} = 24.4 \text{ mA/cm}^2$, and $\text{FF} = 69.8\%$, $R_S = 4.1 \Omega\text{-cm}^2$, $R_{SH} = 1010 \Omega\text{-cm}^2$, $J_0 = 1.6 \times 10^{-7} \text{ mA/cm}^2$, and $A = 1.65$, where “ J_0 ” and “ A ” are reverse saturation current and diode ideality factor. In this device, we optimized the sputtered CdS layer (55–60 nm thick) using 1% oxygen/argon sputter gas²⁵ followed by 2.1 μm thick CdTe sputtered in pure argon. With the incorporation of oxygen in CdS, the window layer becomes more resistant to interdiffusion than when grown in an oxygen-free ambient such that it reduces consumption of CdS during high temperature activation and offers better control of the CdS/CdTe interfacial interdiffusion.^{25–27}

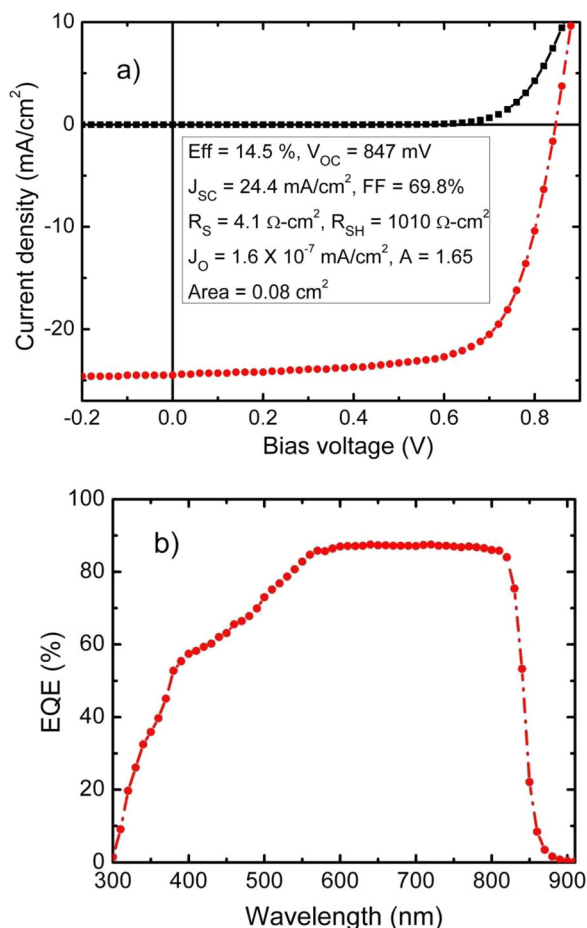


FIG. 7. (a) J-V and (b) EQE data of the best sputtered CdS/CdTe solar cell grown on commercial $\text{SnO}_2:\text{F}/\text{SnO}_2$ -coated soda-lime glass superstrates. The device received 30 min activation at 387 °C in dry air and chloride vapors followed by thermally evaporated elemental Cu (3 nm)/Au (30 nm) back contacts and diffusion at 150 °C.

The J-V characteristic and external quantum efficiency (EQE) of the high efficiency sputtered CdS/CdTe cell are shown in Figures 7(a) and 7(b). The device shows very high current at forward bias (i.e., no roll-over) indicating that the incorporation of oxygen did not degrade the main junction. However, the optical band gap was slightly reduced for the CdS sputtered at 270 °C in 1% oxygen ambient.^{25,28} The sputtered cell exhibited very good EQE response near the CdTe band edge even though the absorber layer is only 2.1 μm thick. However, with a starting CdS layer thickness of 55–60 nm, the EQE still showed a 25%–30% absorption loss in the region from 400 to 550 nm indicating that the oxygenated CdS limited the interdiffusion during the heat-treatment step.

IV. CONCLUSIONS

We have optimized the CdCl_2 activation process for sputtered CdS/CdTe cells on soda-lime glass at activation temperatures from 370 to 440 °C. The optimum annealing time follows an inverse Arrhenius behavior with activation time as short as 20 s at 440 °C. We find that the activation can be described with a single activation energy, $E_a = 1.84 \pm 0.05 \text{ eV}$, and note that this is consistent with the activation energy of sulfur diffusion into polycrystalline CdTe. Activation temperatures above 400 °C yield somewhat lower initial efficiencies than temperatures below 400 °C for our sputtered cells even when the duration is optimized. The higher-temperature-activated devices show good J_{SC} but relatively lower FF and V_{OC} . The somewhat poorer optimized performance after higher temperature activation probably arises from larger numbers of point defects created at these temperatures and poorer interfaces. However, 300-hrs accelerated stressing of cells activated at 430 °C and 440 °C yielded improved cell performance parameters indicating that the low-temperature heat treatment at $\sim 85 \text{ °C}$ can facilitate the reduction of the defects introduced by higher temperature activation. As a result, nearly 10%–15% improvement in FF and V_{OC} was realized and hence the efficiency increased by more than 20% for these cells. Further study is underway to identify the micro-structural changes that occur during high temperature activation and ALT.

We find also that the use of 1% O_2 in Ar as the sputtering gas during CdS deposition limits the junction interdiffusion and facilitates further improvement in the performance of sputtered CdS/CdTe cells. Using commercial $\text{SnO}_2:\text{F}/\text{SnO}_2$ -coated low-iron, soda-lime glass as the superstrate, we have achieved 14.5% efficiency for small-area, sputtered devices.

ACKNOWLEDGMENTS

The Authors would like to thank Dr. David Strickler from NSG (Pilkington NA) Toledo, OH, for supplying low-iron, $\text{SnO}_2:\text{F}$ -coated, soda-lime glass substrates. This work was partially supported by the DOE University PV Process and Product Development Program under Contract No. DE-FG36-08GO18067.

¹P. V. Meyers, C. H. Liu, and T. J. Frey, U.S. patent 4,873,198 (10 October 1989).

²B. E. McCandless, L. V. Moulton, and R. W. Birkmire, *Prog. Photovoltaics* **5**, 249 (1997).

- ³K. V. Krishna and V. Dutta, *Thin Solid Films* **450**, 255 (2004).
- ⁴B. E. McCandless and J. R. Sites, *Handbook of Photovoltaic Science and Engineering*, edited by A. Luque and S. Hegedus (John Wiley & Sons, New York, 2003), p. 617.
- ⁵J. P. Enriquez and X. Mathew, *J. Mater. Sci.: Mater. Electron.* **16**, 617 (2005).
- ⁶J. Krustok, V. Valdna, K. Hjelt, and H. Collan, *J. Appl. Phys.* **80**, 1757–1762 (1996).
- ⁷S. A. Ringel, A. W. Smith, M. H. MacDougal, and A. Rohatgi, *J. Appl. Phys.* **70**, 881 (1991).
- ⁸M. Burgelman, *Thin Film Solar Cells: Fabrication, Characterization and Applications*, edited by J. Poortmans and V. Arkhipov (John Wiley & Sons, New York, 2006), p. 277.
- ⁹A. Romeo, M. Terheggen, D. Abou-Ras, D. L. Batzner, F. J. Haug, M. Kalin, D. Rudmann, and A. N. Tiwari, *Prog. Photovoltaics* **12**, 93 (2004).
- ¹⁰V. V. Plotnikov, D. Kwon, K. A. Wieland, and A. D. Compaan, in *Proceedings of the 34th IEEE Photovoltaic Specialists Conference* (Philadelphia, PA, 2009), pp. 1435–1438.
- ¹¹A. Gupta, V. Parikh, and A. D. Compaan, *Sol. Energy Mater. Sol. Cells* **90**, 2263 (2006).
- ¹²N. R. Paudel, K. A. Wieland, M. Young, S. Asher, and A. D. Compaan, *Prog. Photovoltaics* **22**, 107 (2014).
- ¹³N. R. Paudel, K. A. Wieland, and A. D. Compaan, *Sol. Energy Mater. Sol. Cells* **105**, 109 (2012).
- ¹⁴B. E. McCandless, M. G. Engelmann, and R. W. Birkmire, *J. Appl. Phys.* **89**, 988 (2001).
- ¹⁵M. D. Abramoff, P. J. Magalhaes, and S. J. Ram, *Biophoton. Int.* **11**, 36 (2004).
- ¹⁶N. R. Paudel, K. A. Wieland, and A. D. Compaan, *Mater. Res. Soc. Symp. Proc.* **1323**, 834 (2011).
- ¹⁷C. D. Geddes, *Reviews in Fluorescence 2009* (Springer, New York, 2011).
- ¹⁸H. R. Moutinho, R. G. Dhere, M. M. Al-Jassim, D. H. Levi, and L. L. Kazmerski, *J. Vac. Sci. Technol. A* **17**, 1793 (1999).
- ¹⁹D. Kuciauskus, J. N. Duenow, A. Kanevce, J. V. Li, M. R. Young, P. Dippo, and D. H. Levi, in *Proceedings of the 38th IEEE Photovoltaic Specialists Conference* (Austin, TX, 2012), pp. 1721–1726.
- ²⁰S. Cosap, *Principles of Electronic Materials and Devices*, 3rd ed. (McGraw-Hill, New York, 2006).
- ²¹D. W. Lane, J. D. Painter, M. A. Cousins, G. J. Conibeer, and K. D. Rogers, *Thin Solid Films* **431–432**, 73 (2003).
- ²²J. Britt and C. Ferekides, *Appl. Phys. Lett.* **62**, 2851 (1993).
- ²³X. Wu, *Sol. Energy* **77**, 803 (2004).
- ²⁴A. Gupta and A. D. Compaan, *Appl. Phys. Lett.* **85**, 684 (2004).
- ²⁵N. R. Paudel and Y. Yan, *Thin Solid Films* **549**, 30 (2013).
- ²⁶D. Albin, Y. Yan, and M. M. Al-Jassim, *Prog. Photovoltaics* **10**, 309 (2002).
- ²⁷Y. Yan, D. Albin, and M. M. Al-Jassim, *Appl. Phys. Lett.* **78**, 171 (2001).
- ²⁸A. Gupta, K. Allada, S. H. Lee, and A. D. Compaan, *Mater. Res. Soc. Symp. Proc.* **763**, B8.9.1 (2003).